



ARTICLE

Feasibility study of ^{68}Ga -labeled CAR T cells for in vivo tracking using micro-positron emission tomography imaging

Xin-yu Wang¹, Yan Wang^{2,3}, Qiong Wu¹, Jing-jing Liu¹, Yu Liu¹, Dong-hui Pan¹, Wei Qi⁴, Li-zhen Wang¹, Jun-jie Yan¹, Yu-ping Xu¹, Guang-ji Wang⁵, Li-yan Miao^{2,3}, Lei Yu⁴ and Min Yang¹

Clinical tracking of chimeric antigen receptor (CAR) T cells in vivo by positron emission tomography (PET) imaging is an area of intense interest. But the long-lived positron emitter-labeled CAR T cells stay in the liver and spleen for days or even weeks. Thus, the excessive absorbed effective dose becomes a major biosafety issue leading it difficult for clinical translation. In this study we used ^{68}Ga , a commercially available short-lived positron emitter, to label CAR T cells for noninvasive cell tracking in vivo. CAR T cells could be tracked in vivo by ^{68}Ga -PET imaging for at least 6 h. We showed a significant correlation between the distribution of ^{89}Zr and ^{68}Ga -labeled CAR T cells in the same tissues (lungs, liver, and spleen). The distribution and homing behavior of CAR T cells at the early period is highly correlated with the long-term fate of CAR T cells in vivo. And the effective absorbed dose of ^{68}Ga -labeled CAR T cells is only one twenty-fourth of ^{89}Zr -labeled CAR T cells, which was safe for clinical translation. We conclude the feasibility of ^{68}Ga instead of ^{89}Zr directly labeling CAR T cells for noninvasive tracking of the cells in vivo at an early stage based on PET imaging. This method provides a potential solution to the emerging need for safe and practical PET tracer for cell tracking clinically.

Keywords: CAR T; Gallium-68; Zirconium-89; positron emission tomography; cell tracking; noninvasive imaging

Acta Pharmacologica Sinica (2021) 42:824–831; <https://doi.org/10.1038/s41401-020-00511-5>

INTRODUCTION

Tumor immunotherapy has become a clinical treatment for a variety of tumors due to its significant efficacy [1, 2]. Chimeric antigen receptor (CAR) T cells play an important role in tumor immunotherapy [3]. Viachimeric synthetic receptors, T cells can be redirected to cancer cell surface antigens to kill target cancer cells [4]. In the past few decades, CAR T cell therapy has made significant progress, especially in terms of the clinical success of the use of CD19-CAR T cells for treatment of refractory B-cell malignancies [5, 6], leading to a large number of clinical studies about the use of CAR T cells for tumor treatment. Many CD19-CAR T cell products are undergoing clinical trials; however, only Kymriah and Yescarta were approved by the FDA in 2017 for the treatment of pediatric patients and young adults with refractory or relapsed (R/R) B cell precursor acute lymphoblastic leukemia and adult patients with R/R large B cell lymphoma, respectively [7]. For example, in a CD19-CAR T cell therapeutic trial, the total incidence of cytokine release syndrome (cytokine release syndrome, CRS) events was 35%–93%, while the total incidence of CAR T-related neurotoxic events was 19%–64%, resulting in patient death in severe cases [8, 9]. Unlike the case with conventional drugs, the pharmacological concepts of absorption, distribution, metabolism, and excretion do not fit the pharmacokinetics of CAR T cells,

which are a “living” drug. There is increasing evidence of a positive relationship between CAR T cell exposure and clinical efficacy [10–12]. Therefore, prior to clinical CAR T cell therapy, visualization of the CAR T cell distribution process after administration and testing of the spatiotemporal distribution and homing kinetics in vivo will be very helpful to evaluate tumor treatment effects and toxic side effects in advance [9, 13, 14].

Various imaging modalities have been used to track infused cells in vivo, including bioluminescence imaging with the use of luciferase reporter genes [15] and magnetic resonance imaging with transfection of nanoparticles or emulsions [16]. However, the limited tissue penetration of light or low sensitivity restricts their clinical applications. Thus, radionuclide-based single-photon emission computed tomography (SPECT) and positron emission tomography (PET) methods have been used for cell tracking, as they have excellent tissue penetration and sensitivity [17–19]. ^{111}In -oxine has been utilized for clinical tracking of various types of cells by SPECT scanning, which can continuously monitor labeled cells for 5–7 days [20, 21]. ^{89}Zr -oxine was also used for cell tracking by PET imaging [22–25]. Although long-term tracking of CAR T cells will provide more information on homing and distribution dynamics, radionuclides such as ^{89}Zr remain in the liver, spleen, and lung for days or even weeks. Thus, the excess

¹NHC Key Laboratory of Nuclear Medicine, Jiangsu Key Laboratory of Molecular Nuclear Medicine, Jiangsu Institute of Nuclear Medicine, Wuxi 214063, China; ²Department of Clinical Pharmacology, The First Affiliated Hospital of Soochow University, Suzhou 215006, China; ³Institute for Interdisciplinary Drug Research and Translational Sciences, College of Pharmaceutical Sciences, Soochow University, Suzhou 215123, China; ⁴School of Chemistry and Molecular Engineering, East China Normal University, Shanghai Unicar-Therapy Bio-medicine Technology Co., Ltd., Shanghai 200062, China and ⁵Key Laboratory of Drug Metabolism and Pharmacokinetics, State Key Laboratory of Natural Medicines, China Pharmaceutical University, Nanjing 210009, China

Correspondence: Li-yan Miao (miaolysuzhou@163.com) or Lei Yu (lylh188@163.com) or Min Yang (yangmin@jnsim.org)

These authors contributed equally: Xin-yu Wang, Yan Wang

Received: 14 May 2020 Accepted: 17 August 2020

Published online: 8 September 2020

absorbed radiation dose makes clinical translation of this method difficult. Alternatively, radionuclides with a short half-life, such as ^{18}F , have been developed for cell tracking by reporter gene transfection, including [^{18}F] FHBG [26], [^{18}F] FBEM [27], and [^{18}F] DCFPyL [28]. This method requires additional gene transfection procedures, which remains a biosafety issue for clinical translation. Furthermore, it cannot be universally used for different types of CAR T cells. The sensitivity is also insufficient for early tracking.

Herein, we report CAR T cells directly labeled with ^{68}Ga -oxine and the feasibility of their use for in vivo tracking by PET imaging. CAR T cells directly labeled with ^{89}Zr -oxine were used as a long-term control. We applied this strategy in mice for CAR T cell tracking by PET imaging and verified the cell distribution ex vivo.

MATERIALS AND METHODS

Materials

8-Hydroxyquinoline (oxine), sodium citrate, NaOAc, Na_2CO_3 , and 2-[4-(2-hydroxyethyl)piperazin-1-yl]ethanesulfonic acid (HEPES) solution were purchased from Sigma Aldrich (St Louis, MO). ^{89}Zr -oxalate was obtained from BV Cyclotron VU (The Netherlands). $^{68}\text{Ga}^{3+}$ solution was eluted from a $^{68}\text{Ge}/^{68}\text{Ga}$ generator (ITG, Germany) with 4 mL of 0.05 mol/L HCl (Merck, Germany), from which the 0.5 mL fraction with the highest radioactivity was used for further experiments.

Cell culture

The human Burkitt's lymphoma cell line Raji-luc was purchased from Biocytogen (Beijing, China). CD19-CAR T cells were obtained from Shanghai Unicar Biomed-Pharmaceutical Technology Co., Ltd. The human chronic myelogenous leukemia cell line K562 was originally purchased from ATCC (Manassas, VA). The K562 cell line was transduced with a lentiviral vector encoding the human CD19 gene and a firefly luciferase reporter gene to generate the CD19-K562-luc cell line. CD19-K562-luc and Raji-luc cells were cultured at 37 °C with 5% CO_2 in ATCC modified RPMI-1640 medium (Gibco) containing 10% fetal bovine serum (Gibco) and 1% penicillin-streptomycin.

Animals

In vivo analysis of CAR T cell function was performed by establishing xenograft models with NOD/ShiLJ/Gpt-Prkdc^{em26Cd52}/J2rg^{em26Cd22}/Gpt (NSG, NBRI) mice. For the disseminated disease model, mice were injected intravenously with 5×10^6 human Burkitt's lymphoma (Raji)-luc cells. For the localized disease model, mice were engrafted subcutaneously (s.c.) on the right back with 5×10^6 CD19-K562-luc cells. To verify the success of the tumor model, mice received 15 mg/mL luciferin-D working solution through intraperitoneal injection and were imaged using an IVIS Lumina LT in vivo imaging system (PerkinElmer). Kunming (KM) mice were obtained from CAVENS (Changzhou, China). All animal experiments were conducted by following the National Institutes of Health guidelines for the care and use of laboratory animals and approved by the Institutional Animal Care and Ethics Committee of Jiangsu Institute of Nuclear Medicine (Wuxi, China).

Radiolabeling of CAR T cells

For ^{68}Ga -oxine labeling, the pH of the $^{68}\text{Ga}^{3+}$ solution was adjusted to 5–6 using 1 M NaOAc, and then the solution was mixed with 20 μg oxine dissolved in 20 μL 10% acetic acid. The reaction lasted for 15 min at room temperature. For ^{89}Zr -oxine labeling, the pH of the $^{89}\text{Zr}^{4+}$ solution was adjusted to 7 using 1 M Na_2CO_3 and 0.2 M HEPES buffer. Then, 20 μg oxine dissolved in 20 μL 10% acetic acid was added to the $^{89}\text{Zr}^{4+}$ solution and allowed to react for 15 min at room temperature. For radio labeled CAR T cells, 1×10^5 CAR T cells were incubated with 1.11 MBq ^{68}Ga - or ^{89}Zr -oxine solution at room temperature for 10 min and then centrifuged at 2000 rpm for 5 min. Finally, the ^{68}Ga - and

^{89}Zr -CAR T cells were washed 3 times with PBS buffer. The intracellular and supernatant radioactivity was measured by a γ -counter (Perkin Elmer, USA). The cell viability and cell count before and after radiolabeling were detected using a fully automated cell counter (BodBoge, Shenzhen, China). The stability of the radiolabeled CAR T cells in cell culture medium (10% serum) was evaluated using thin layer chromatography with a radioactivity detector (radio-TLC, Bioscan, USA); the mobile phase was 0.15 M sodium citrate solution, and the plates consisted of glass microfiber chromatography paper impregnated with silica gel.

PET scan

All PET scans were performed on an Inveon microPET scanner (Siemens Solutions, Germany). KM, NSG, CD19-K562-luc xenograft model and Raji-luc model mice were intravenously injected with 1×10^6 ^{68}Ga - or ^{89}Zr -radiolabeled CAR T cells via the tail vein. The radioactivity of each mouse was 185 KBq. For ^{68}Ga -CAR T cell imaging, the 1-h dynamic PET scan was started immediately after intravenous injection, and 10-min-long static PET scans were conducted at 2, 4, and 6 h p.i. For ^{89}Zr -CAR T cell imaging, the 2-h dynamic PET scan was started immediately after intravenous injection, and 10-min- or 20-min-long static PET scans were performed at 4, 6, 24, 48, 72, 90, 112, 140, 168, and 260 h p.i.

Image data analysis

PET images were reconstructed using a 3-dimensional ordered subset expectation maximum algorithm, and the image data were analyzed by ASIPro software. The major organs and tissues of each mouse, such as the lung, liver, and spleen, were delineated manually on the images as the regions of interest (ROIs). The image-derived percentage injected dose per gram (%ID/g) was calculated for each ROI and used as the indicator for the quantification of radioactivity uptake. Furthermore, by considering the effect of body weight, the standardized uptake values were also calculated and used as another indicator. The %ID/g and SUV can be obtained using the following equations:

$$\%ID/g = \text{ROI activity concentration (KBq/mL)} / \text{Total injected activity (KBq)} * 100$$
$$\text{SUV} = \text{ROI activity concentration (KBq/mL)} / \text{Total injected activity (KBq)} / \text{body weight (g)}$$

Pharmacokinetics study

The pharmacokinetics of ^{89}Zr -labeled CAR T cells were investigated in NSG mice, a CD19-K562-luc xenograft mouse model and a Raji mouse model after intravenous injection with 1×10^6 ^{89}Zr -CAR T cells. ^{68}Ga -CAR T cells were intravenously injected into NSG mice only. The radioactivity of each mouse was 185 KBq. Blood samples were collected from the tail and weighed at various times after i.v. injection. The radioactivity of blood samples was determined with a γ counter and normalized to the %ID/g. The area under the curve (AUC) for blood uptake (%ID/g) versus time was calculated using the noncompartment fitting method with DAS software (version 2.0).

Ex vivo biodistribution

KM mice were intravenously injected with 1×10^6 ^{68}Ga -CAR T cells or ^{89}Zr -CAR T cells. Then, the mice injected with ^{68}Ga -labeled CAR T cells were sacrificed at 0.5, 1, 2, and 4 h p.i., while the mice injected with ^{89}Zr -labeled CAR T cells were sacrificed at 0.5, 2, and 4 h p.i. Samples of major organs and tissues, including blood, brain, liver, heart, spleen, lung, kidney, muscle, and knee, were removed and weighed. The radioactivity of each sample was measured using a γ -counter, and then the %ID/g per organ was calculated.

Absorbed dose estimates

The organ activity and concentration data were obtained by drawing the ROIs on the PET images of NSG mice for the following

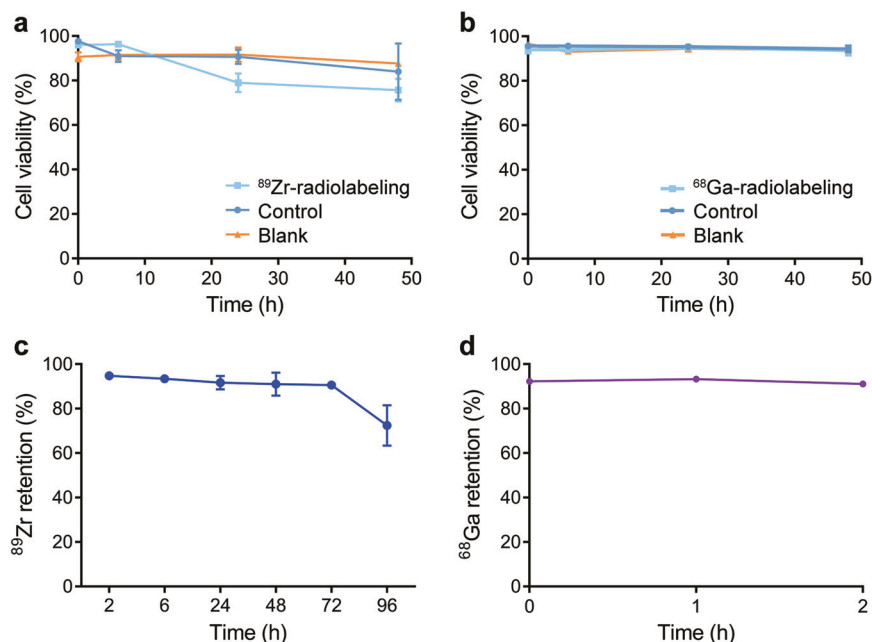


Fig. 1 Cell viability and radionuclides retention of radiolabeled CAR T cells. In vitro cell viability of ^{89}Zr -labeled CAR T cells (a) and ^{68}Ga -labeled CAR T cells (b) compared with that of the unlabeled control. Blank represents cells subjected to the labeling process without radionuclides. c ^{89}Zr retained in CAR T cells after 96 h. d ^{68}Ga retained in CAR T cells after 2 h. Values are expressed as the means \pm SD ($n = 3$)

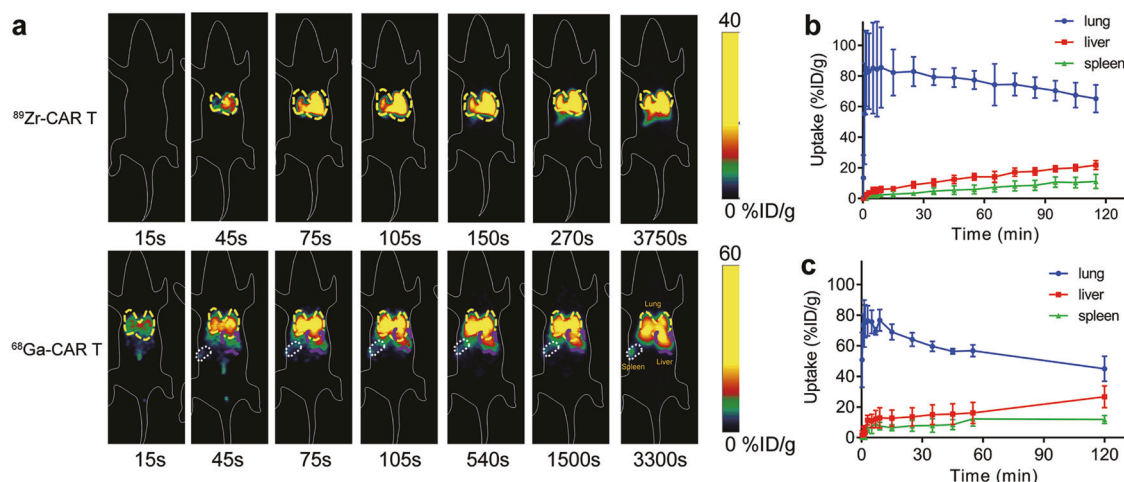


Fig. 2 In vivo tracking of radiolabeled CAR T cells by dynamic PET scan. a Representative coronal PET images of NSG mice injected with ^{89}Zr -labeled CAR T cells and ^{68}Ga -labeled CAR T cells. b, c Time activity curve generated from dynamic PET images of NSG mice injected with ^{89}Zr -labeled CAR T cells (b, $n = 4$) and ^{68}Ga -labeled CAR T cells (c, $n = 3$)

organs/tissues: lung, liver, spleen, blood (left ventricular chamber), muscle, and other organs. The organ residence times of the mice could be fitted with PMOD (version 3.8). Subsequently, by referring to the calculation method in the OLINDA software handbook, the residence time for each organ in the mouse can be extrapolated based on the adult male (73 kg). The remainder of the body residence time was determined based on the maximum theoretical residence time minus the sum of the residence times observed in the organs. The human dosimetry estimates were obtained from the residence times using OLINDA/EXM (version 2.0) software with the adult male model.

Statistical analysis

Data are expressed as the mean \pm SD. Student's *t* test and one-way ANOVA with Tukey's post hoc test were used for the significant difference determination, and Pearson's coefficient was used to

evaluate the correlation. Differences were considered statistically significant when the *P* value < 0.05 . Statistical analysis was performed with SPSS 19.0, and figures were plotted with GraphPad Prism 7.

RESULTS

Radiolabeling of CAR T cells

^{89}Zr -oxine was obtained by mixing neutralized $^{89}\text{Zr}(\text{oxalate})_4$ with 8-hydroxyquinoline. The radiochemical yield was greater than 90%. ^{68}Ga -oxine was obtained by mixing $^{68}\text{GaCl}_3$ solution with 8-hydroxyquinoline at a pH value between 5 and 6. The radiochemical yield was also greater than 90%. ^{89}Zr -oxine or ^{68}Ga -oxine was added to CAR T cells immediately and incubated at room temperature for radiolabeling of the cells. After centrifugation and washing 3 times, the CAR T cells were used for further

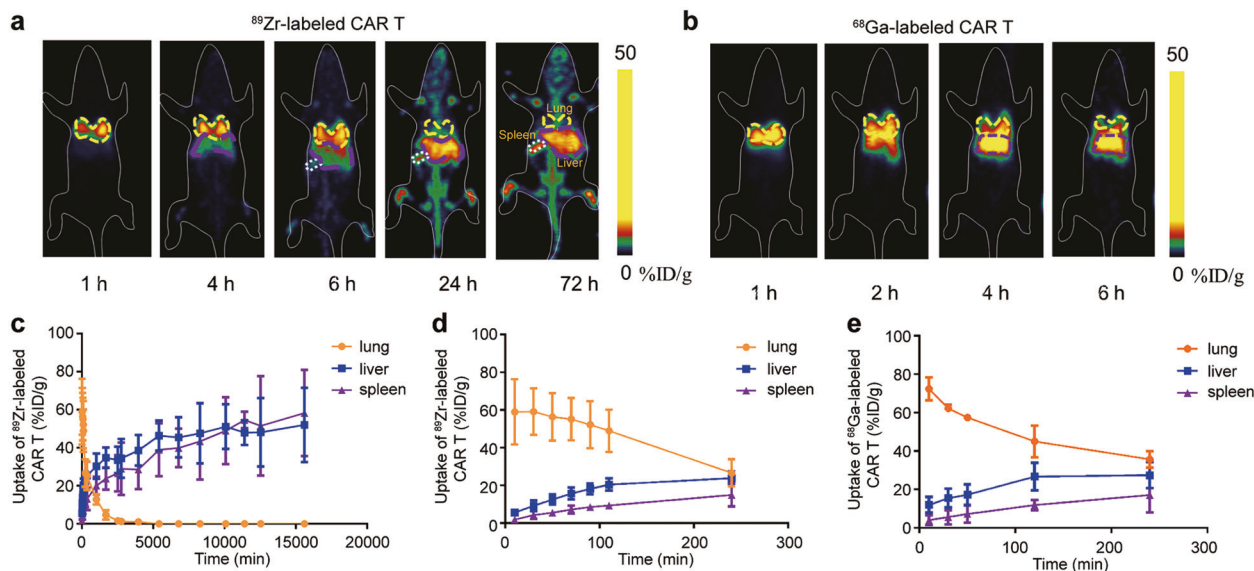


Fig. 3 In vivo tracking of radiolabeled CAR T cells in NSG mice by static PET scan. **a** Representative coronal PET images of mice injected with ^{89}Zr -labeled CAR T cells at various time points within 72 h p.i. **b** Representative coronal PET images of mice injected with ^{68}Ga -labeled CAR T cells at various time points within 6 h p.i. **c** Time-dependent ^{89}Zr -labeled CAR T cell uptake percentage in the lung, liver, and spleen within 260 h ($n = 4$). **d** Time-dependent ^{89}Zr -labeled CAR T cell and **e** ^{68}Ga -labeled CAR T cell uptake percentages in the lung, liver, and spleen within 4 h ($n = 4$ for ^{89}Zr -labeled CAR T cells, and $n = 3$ for ^{68}Ga -labeled CAR T cells). Values are expressed as the means \pm SD

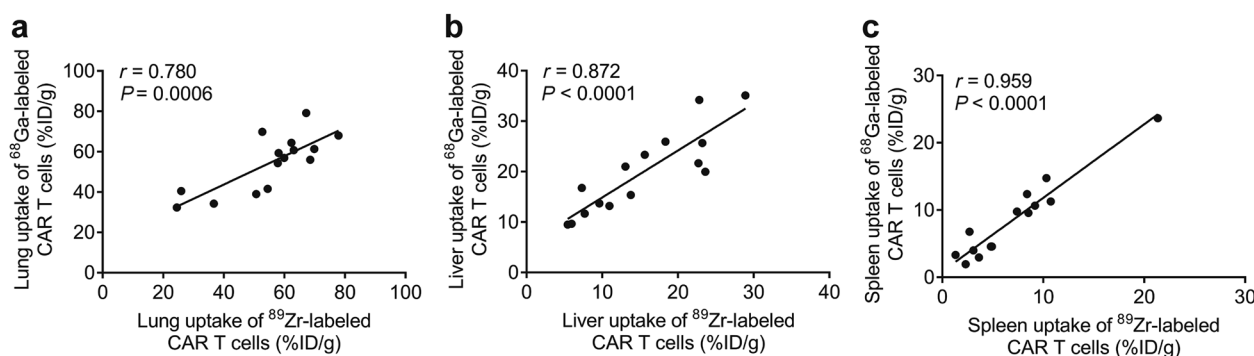


Fig. 4 Correlation between tissue uptake of ^{89}Zr - and ^{68}Ga -labeled CAR T cells. Pearson correlation analysis of ^{89}Zr -labeled CAR T cells vs ^{68}Ga -labeled CAR T cells in the lungs (a), liver (b), and spleen (c) within 4 h

study. As shown in Fig. 1a, the viability of the CAR T cells changed slightly after radiolabeling with ^{89}Zr -oxine. The viability of ^{89}Zr -labeled CAR T cells was $\sim 80\%$ at 24 h and 48 h post radiolabeling. Meanwhile, for ^{68}Ga -labeled CAR T cells, the viability remained above 95% in 48 h (Fig. 1b). For ^{89}Zr -labeled cells, more than 90% of the radioactivity was retained after 72 h, which represented one half-life of the radionuclide ^{89}Zr , and the radioactivity decreased to $\sim 70\%$ at 96 h after radiolabeling (Fig. 1c). To study the intracellular stability of ^{68}Ga and ^{89}Zr , the retention of radioactivity in cells was tested. More than 90% of ^{68}Ga was retained in CAR T cells after 2 h, which represented two half-lives of the radionuclide ^{68}Ga (Fig. 1d).

PET imaging

After intravenous injection of radiolabeled CAR T cells, dynamic PET scans and static scans were performed to obtain PET images at various times p.i. PET images showed similar results for ^{89}Zr and ^{68}Ga -labeled CAR T cells in vivo within the first 6 h in all four types of mice. In NSG mice, ^{89}Zr - and ^{68}Ga -labeled CAR T cells were initially distributed in the lungs within the first several minutes post injection and gradually migrated to the spleen and liver (Figs. 2 and 3). At 24 h and 72 h p.i., ^{89}Zr -labeled CAR T cells remained mainly in the spleen and liver. These results are

consistent with previous reports of ^{89}Zr -labeled CAR T cells [23, 29]. The Pearson correlation analysis in Fig. 4 shows significant correlations between the distribution of ^{89}Zr and ^{68}Ga -labeled CAR T cells in the lungs ($r = 0.780$, $P = 0.0006$), liver ($r = 0.872$, $P < 0.0001$) and spleen ($r = 0.959$, $P < 0.0001$) within 4 h p.i. PET imaging of CD19-K562-luc and Raji model mice (Supplementary Fig. S1) showed that the tumor uptake of radiolabeled CAR T cells was slow, and no significant accumulation was found within 4 h ($< 1\% \text{ID/g}$). Thus, ^{89}Zr -labeled CAR T cells were used to determine the relationship between the early-stage and long-term fate.

Pharmacokinetics of radiolabeled CAR T cells

As shown in Fig. 5a, b, the clearance of ^{89}Zr -labeled CAR T cells was different in tumor-free mice and tumor-bearing mice. The mean half-life ($t_{1/2}$) of ^{89}Zr -labeled CAR T cells in NSG mice and the CD19-K562-luc model mice was 211 and 204 min, respectively, whereas it was prolonged by 790 min in the Raji model mice. The AUC analysis also confirmed that exposure to radiolabeled CAR T cells in the blood of tumor-bearing mice was significantly higher than that of NSG mice (Fig. 5c). For NSG, CD19-K562-luc, and Raji model mice, the mean AUCs of the blood pharmacokinetics of ^{89}Zr -labeled CAR T cells were 1854, 5306, and 17178 $\% \text{ID/g} \cdot \text{min}$, respectively. Pearson correlation analysis revealed a high correlation between blood

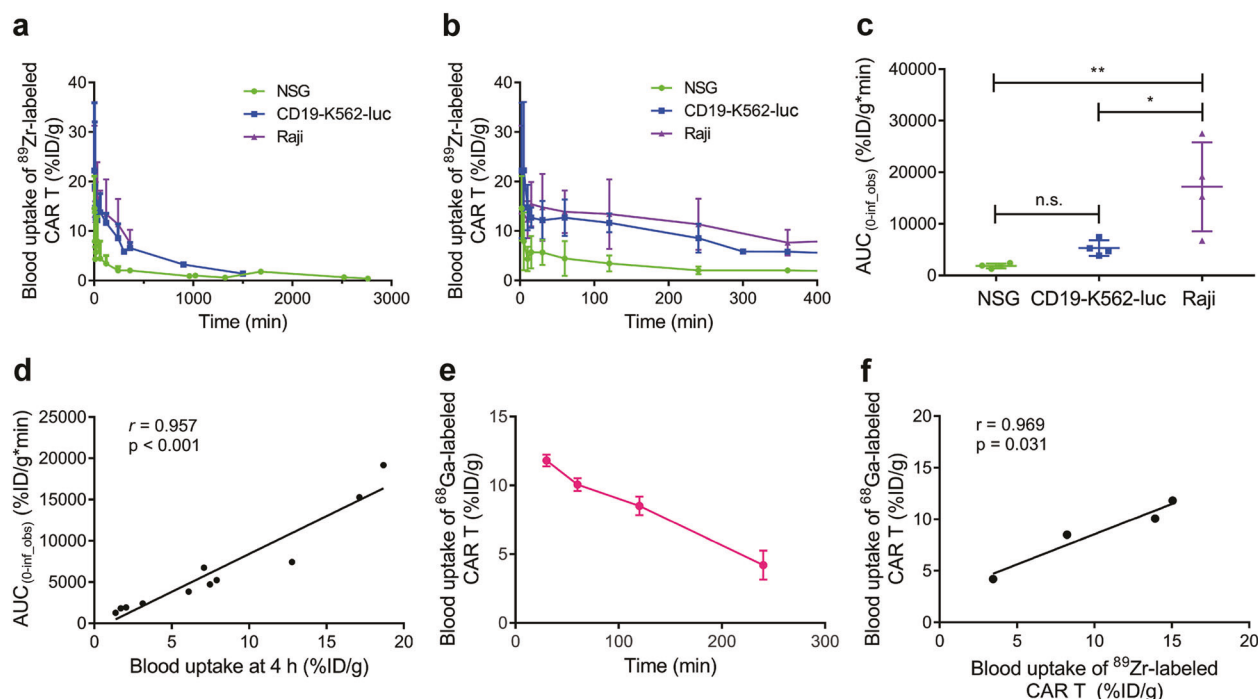


Fig. 5 Pharmacokinetics of radiolabeled CAR T cells. PK curve of ^{89}Zr -labeled CAR T cells at various time points within 46 h p.i. (a) and within 6 h p.i. (b) in NSG, CD19-K562, and Raji mouse models. c AUC_(0-inf_obs) for the blood uptake of ^{89}Zr -labeled CAR T cells. d Pearson correlation analysis of the AUC_(0-inf_obs) of blood pharmacokinetics vs the blood uptake dose at 4 h p.i. in the NSG, CD19-K562, and Raji models. e Blood uptake of ^{68}Ga -labeled CAR T cells within 4 h p.i. in NSG mice ($n = 3$). f Pearson correlation analysis of the blood uptake of ^{68}Ga -labeled and ^{89}Zr -labeled CAR T cells. The correlation analysis was based on the blood uptake in NSG mice for both ^{68}Ga -labeled and ^{89}Zr -labeled CAR T cells. Values are expressed as the means \pm SD ($n = 4$). * $P < 0.05$, ** $P < 0.01$, ^{n.s.} $P \geq 0.05$ analyzed by one-way ANOVA with Tukey's post hoc test

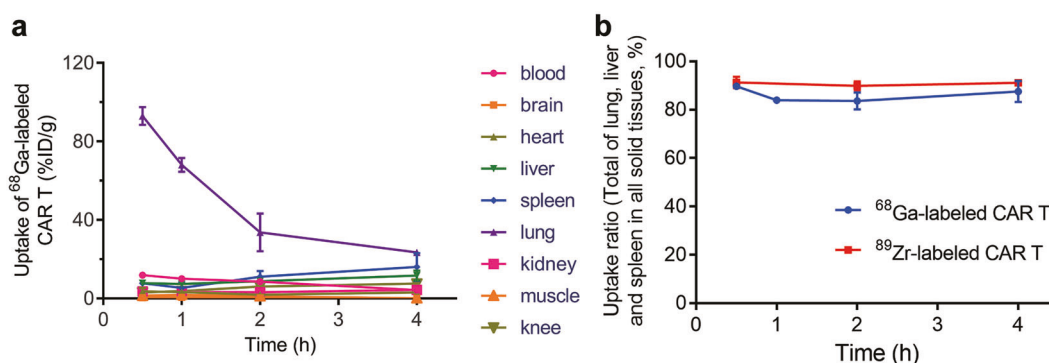


Fig. 6 Ex vivo biodistribution of radiolabeled CAR T cells in KM mice. a Biodistribution of ^{68}Ga -labeled CAR T cells within 4 h p.i. in blood, brain, heart, liver, spleen, lung, kidney, muscle, and knee. b Total biodistribution of ^{68}Ga -/ ^{89}Zr -labeled CAR T cells in the lung, liver and spleen among all solid tissues within 4 h p.i. Values are expressed as the means \pm SD ($n = 3$)

uptake at 4 h p.i. and the AUC_(0-∞) of radiolabeled CAR T cells (Fig. 5d). The pharmacokinetics of ^{68}Ga -labeled CAR T cells were also investigated in NSG mice (Fig. 5e). A high correlation for blood uptake between ^{68}Ga -labeled CAR T cells and ^{89}Zr -labeled CAR T cells within 4 h was also found (Fig. 5f).

Ex vivo biodistribution

KM mice were sacrificed at various times after radiolabeled CAR T cell injection for the ex vivo biodistribution study (Fig. 6). A very rapid reduction in lung uptake was found within the first 2 h in mice treated with radiolabeled CAR T cells. The lung uptake decreased from 93.0% ID/g to 33.7% ID/g for ^{68}Ga -labeled CAR T cells. At the same time, liver and spleen uptake increased as lung uptake decreased. The total accumulation of ^{68}Ga -labeled CAR T cells in the lungs, liver and spleen within all solid tissues reached more than 80% 4 h after injection. Thus, for other organs,

such as the brain, heart and kidney, few of the ^{68}Ga -labeled CAR T cells were distributed within them. The ^{89}Zr -labeled CAR T cells also remained in the lungs, liver and spleen within the first 4 h similarly to the ^{68}Ga -labeled CAR T cells. We also compared the ex vivo distribution and PET imaging results of ^{89}Zr -labeled CAR T cells in KM mice. To eliminate the body weight effect, we used SUV as the indicator. The SUV of the lung, liver and spleen at 4 h p.i. are shown in Supplementary Fig. S2. The distribution was similar in the lung and liver, while spleen uptake ex vivo was slightly higher than that observed during PET imaging.

Absorbed dose estimates

The estimations of the human absorbed doses to normal tissues based on PET imaging of ^{89}Zr - and ^{68}Ga -labeled CAR T cells in NSG mice are summarized in Table 1. The calculated dosimetry data showed that the total whole-body effective dose from ^{68}Ga -

Table 1. Absorbed dose estimates for ^{89}Zr -labeled CAR T cells and ^{68}Ga -labeled CAR T cells in selected organs

Target organ	Effective dose (mSv/MBq)	
	^{89}Zr	^{68}Ga
Adrenals	3.13×10^{-2}	2.13×10^{-4}
Brain	3.01×10^{-4}	4.63×10^{-6}
Esophagus	4.23×10^{-2}	6.58×10^{-4}
Eyes	0.00×10^{00}	0.00×10^{00}
Gallbladder wall	1.43×10^{-2}	1.45×10^{-4}
Left colon	4.54×10^{-2}	3.20×10^{-4}
Small intestine	3.73×10^{-3}	2.81×10^{-5}
Stomach wall	2.25×10^{-1}	2.23×10^{-3}
Right colon	2.55×10^{-2}	2.17×10^{-4}
Rectum	2.33×10^{-3}	1.55×10^{-5}
Heart wall	8.80×10^{-3}	1.75×10^{-4}
Kidneys	1.65×10^{-2}	1.18×10^{-4}
Liver	1.41×10^{-1}	3.60×10^{-3}
Lungs	2.69×10^{-1}	3.50×10^{-2}
Pancreas	1.18×10^{-2}	9.82×10^{-5}
Prostate	5.89×10^{-4}	3.75×10^{-6}
Salivary glands	6.67×10^{-4}	1.15×10^{-5}
Red marrow	6.00×10^{-2}	7.68×10^{-4}
Osteogenic cells	2.78×10^{-3}	3.37×10^{-5}
Spleen	3.65×10^{-1}	8.79×10^{-3}
Testes	6.91×10^{-4}	3.61×10^{-6}
Thymus	5.14×10^{-3}	1.10×10^{-4}
Thyroid	1.46×10^{-2}	3.74×10^{-4}
Urinary bladder wall	2.45×10^{-3}	1.61×10^{-5}
Total Body	1.29×10^{00}	5.30×10^{-2}

labeled CAR T cells was dozens of times lower than that from ^{89}Zr -labeled CAR T cells (1.29 mSv/MBq for ^{89}Zr and 0.053 mSv/MBq for ^{68}Ga). The absorbed effective dose was far less than that received from typical abdominal CT scans. The doses received by the lungs, liver, spleen, and stomach wall were relatively higher than those received by other tissues and organs for both for ^{89}Zr - and ^{68}Ga -labeled CAR T cells.

DISCUSSION

In recent decades, many radionuclides have been used for cell tracking, such as ^{111}In , $^{99\text{m}}\text{Tc}$, ^{89}Zr , ^{68}Ga , ^{64}Cu , and ^{18}F [21, 30–32]. The probe molecules labeled with these radionuclides were designed to directly or indirectly label cells, either by direct loading inside cells or by binding to receptors on the surfaces of cell membranes [33]. The radionuclides used for cell tracking usually need to meet certain conditions, including having the proper positron energy and abundance, convenient and economical availability, simple labeling procedures, minimal effects on cell survival and function, and minimal efflux from cells. ^{68}Ga is a radioisotope with better positron abundance, energy and gamma emission than ^{89}Zr , but its half-life is only 67.7 min. The successful commercialization of the $^{68}\text{Ge}/^{68}\text{Ga}$ generator has also made its use convenient for clinical studies [34]. The use of ^{68}Ga for direct labeling of cells often makes it difficult to track cell distribution in vivo because ^{68}Ga can generally only support PET imaging for a few hours, while cell tracking usually takes several days. For killer T cells such as CAR T cells, cell tracking over several days allows for the observation of accumulation within the solid tumor [23]. However, long-lived radionuclides in CAR T cells remain in the liver

and spleen for days or even weeks, which remains a safety concern for clinical translation. Therefore, we attempted to prepare CAR T cells directly labeled with the ^{68}Ga radioisotope to study the cell tracking ability of PET imaging.

We first studied the process of labeling with ^{68}Ga -oxine in the examined cells. Similar to the ^{89}Zr -oxine complex [24], the ^{68}Ga -oxine complex can be prepared by simply mixing the components in an aqueous solution. The obtained complex can be directly used for cell labeling without further purification. Within the two half-lives of ^{68}Ga , no obvious efflux of ^{68}Ga from cells was found. Moreover, the oxine-mediated direct labeling process is also conducive to the survival of the studied cells, which is consistent with reports in the literature [24]. Furthermore, owing to the short life of ^{68}Ga , ^{68}Ga -labeled CAR T cells showed higher cell viability than ^{89}Zr -labeled CAR T cells. These results indicate that ^{68}Ga -oxine, similar to ^{89}Zr -oxine, can be used for living cell labeling.

We used PET imaging to monitor the distribution behavior of radiolabeled CAR T cells in vivo and perform ex vivo biodistribution tests. Due to the massive difference in the half-lives of ^{68}Ga and ^{89}Zr , ^{68}Ga -labeled CAR T cells were monitored by PET imaging for 6 h, while ^{89}Zr -labeled CAR T cells were monitored for 260 h. The overall biodistribution observed for the ^{89}Zr - and ^{68}Ga -labeled CAR T cells was basically consistent. The cells were first taken up by the lungs and then migrated to the liver and spleen. The in vivo behavior of ^{68}Ga -labeled CAR T cells is also consistent with that of oxine-mediated ^{111}In -labeled and ^{89}Zr -labeled CAR T cells [22, 23]. We performed a Pearson correlation analysis of the in vivo distribution of ^{89}Zr - and ^{68}Ga -labeled CAR T cells based on the PET images, and the results showed that their distribution in vivo was strongly correlated. The blood uptake of ^{89}Zr - and ^{68}Ga -labeled CAR T cells was also found to be highly related. Combining these results, it can be concluded that the use of ^{68}Ga -oxine is completely feasible for cell labeling and short-term imaging of cells in vivo.

Severe combined immuno deficiency mice were selected for the pharmacokinetics study, including Raji Burkitt's lymphoma model, CD19-K562-lucx enograft and NSG mice. The Raji Burkitt's lymphoma model is a human lymphoma xenograft model. CAR T cells first recognize the antigen and then bind tumor cells after entering the body [35]. Because the blood circulation of the Raji model mouse contains a large number of tumor cells, it is apparent that the metabolic clearance of radiolabeled CAR T cells from the blood of the Raji model is significantly lower than that of the CD19-K562-luc and NSG models. The blood clearance half-life was as high as 790 min, which is ~4 times longer than that of the other two models. The CAR T cell-based therapies result in a long clearance time in the blood, which exceeds the tracking period of the ^{68}Ga radioisotope. However, we can see that the early metabolic rate (the first 4 h p.i.) is completely related to the long-term metabolic rate, so we only need to obtain the early distribution data to predict the long-term metabolic process.

The ex vivo biodistribution analysis and PET imaging also confirmed that the majority of the ^{68}Ga -labeled CAR T cells remained in the lung, spleen, and liver 4 h after injection, similar to the ^{89}Zr -labeled CAR T cells. Surprisingly, spleen uptake was slightly higher than liver uptake according to the ex vivo biodistribution, whereas the PET imaging results indicated the opposite. We compared the 4 h p.i. results for ^{89}Zr -labeled CAR T cells in KM mice (Fig. S2), and there was no significant difference between the liver and spleen according to both PET imaging and the ex vivo biodistribution in KM mice. We speculate that the slight difference in the spleen is due to ROI selection. The distribution data obtained from PET images represent the ROI, which is just a slice of the whole organ, whereas the ex vivo distribution represents the whole organ. The cell distribution in the same organ is not homogeneous. Furthermore, the drawing of the ROI for the spleen is difficult because the volume of the spleen is quite small, whereas the liver is large enough to easily select the highly radioactive area. This is a limitation of microPET without computed tomography (CT).

This issue can be easily resolved in clinical translation by fusing PET images and CT images in PET/CT scans. In a previous study, a mismatch of the distribution in the liver and spleen determined by ex vivo biodistribution and PET imaging was also observed [29], similar to our study. The liver uptake of radiolabeled $\gamma\delta$ -T cells was higher than spleen uptake at 168 h p.i. according to PET imaging, whereas the uptake in the liver was lower than that in the spleen according to the ex vivo distribution.

Dosimetry analysis can help predict potential toxicity that may occur in humans and can also help scientists determine the optimized initial dose strategy when needed. The pattern of the absorbed dose values obtained in this study indicates that CAR T cells were located in several tissues. Due to the short half-life of the ^{68}Ga radioisotope, the absorbed dose value produced by ^{68}Ga -labeled CAR T cells in each organ was much lower than that produced by ^{89}Zr -labeled CAR T cells. The total absorbed dose of ^{68}Ga -labeled CAR T cells was only one twenty-fourth of that of ^{89}Zr -labeled CAR T cells. Even in the lung, which had the highest absorbed dose, the absorbed dose was only one-seventh of that resulting from ^{89}Zr -labeled CAR T cells. The great reduction of the systemic absorbed dose can effectively ensure the safety of the irradiation dose used in the clinical translation process of the cell tracking method.

This proof-of-concept study demonstrated that CAR T cells directly labeled with short half-life radionuclides can also be used for in vivo cell tracking by PET imaging. The convenient operation, high feasibility, and low absorbed dose of this method indicate its high potential for clinical translation. In the future, further exploration of the relationships between early PET imaging, metabolic kinetic data and the degree of disease progression and prognosis can provide more support for the clinical translation of this cell tracking method.

CONCLUSION

In summary, we demonstrated the feasibility of the replacement of ^{89}Zr with ^{68}Ga to directly label CAR T cells for in vivo cell tracking by PET imaging. This method can be utilized for cell tracking in the early period post CAR T cell administration. Early observations of the dynamic trafficking of CAR T cells were correlated with the long-term fate of infused CAR T cells in vivo. The accurately quantitated ^{68}Ga -labeled CAR T cells, which were trafficked to organs with low radionuclide exposure, have much better safety profiles than ^{89}Zr -labeled CAR T cells, suggesting that this method can be safely translated to humans. This method provides a potential solution for the emerging need for safe and practical PET tracers for cell tracking in the clinic and deserves further evaluation to determine its behavior in various cell types and animal models.

ACKNOWLEDGEMENTS

We thank financial supports from the Leading technology foundation research project of Jiangsu province (BK20192005), National Natural Science Foundation of China (31971316), National Significant New Drugs Creation Program (2017ZX09304021), Jiangsu Province Foundation (BK20170204), Jiangsu Provincial Medical Innovation Team (CXTDA2017024), 333 Project in Jiangsu Province (BRA2019105), Innovation Capacity Development Plan of Jiangsu Province (BM2018023), and Jiangsu Provincial Key Medical Discipline (ZDXKA2016017).

AUTHOR CONTRIBUTIONS

MY, LYM, LY, and GJW designed the experiments. YW, QW, JLL, DHP, LZW, JYJ, and YPX performed the radiolabeling, microPET imaging, and biodistribution experiments. WQ established the cell lines and animal models. YW, XYW, QW, and JLL analyzed the data. XYW, YW, YL, MY, and LY wrote the manuscript.

ADDITIONAL INFORMATION

The online version of this article (<https://doi.org/10.1038/s41401-020-00511-5>) contains supplementary material, which is available to authorized users.

Competing interests: The authors declare no competing interests.

REFERENCES

1. Khalil DN, Smith EL, Brentjens RJ, Wolchok JD. The future of cancer treatment: immunomodulation, CARs and combination immunotherapy. *Nat Rev Clin Oncol*. 2016;13:273–90.
2. Emens LA, Ascierto PA, Darcy PK, Demaria S, Eggermont AM, Redmond WL, et al. Cancer immunotherapy: opportunities and challenges in the rapidly evolving clinical landscape. *Eur J Cancer*. 2017;81:116–29.
3. June CH, Sadelain M. Chimeric antigen receptor therapy. *N Engl J Med*. 2018;379:64–73.
4. Sadelain M, Rivière I, Riddell S. Therapeutic T cell engineering. *Nature*. 2017;545:423–31.
5. Bach PB, Giralat SA, Saltz LB. FDA approval of tisagenlecleucel: promise and complexities of a \$475 000 cancer drug. *JAMA*. 2017;318:1861–2.
6. Bouchkouj N, Kasamon YL, de Claro RA, George B, Lin X, Lee S, et al. FDA approval summary: axicabtagene ciloleucel for relapsed or refractory large B-cell lymphoma. *Clin Cancer Res*. 2019;25:1702–8.
7. Mullard A. 2017 FDA drug approvals. *Nat Rev Drug Discov*. 2018;17:81–5.
8. Hay KA. Cytokine release syndrome and neurotoxicity after CD19 chimeric antigen receptor-modified (CAR-) T cell therapy. *Br J Haematol*. 2018;183:364–74.
9. Neelapu SS, Tummala S, Kebriaei P, Wierda W, Gutierrez C, Locke FL, et al. Chimeric antigen receptor T-cell therapy—assessment and management of toxicities. *Nat Rev Clin Oncol*. 2018;15:47–62.
10. Ali SA, Shi V, Maric I, Wang M, Stroncek DF, Rose JJ, et al. T cells expressing an anti-B-cell maturation antigen chimeric antigen receptor cause remissions of multiple myeloma. *Blood*. 2016;128:1688–700.
11. Mueller KT, Maude SL, Porter DL, Frey N, Wood P, Han X, et al. Cellular kinetics of CTL019 in relapsed/refractory B-cell acute lymphoblastic leukemia and chronic lymphocytic leukemia. *Blood*. 2017;130:2317–25.
12. Kochenderfer JN, Somerville RP, Lu T, Yang JC, Sherry RM, Feldman SA, et al. Long-duration complete remissions of diffuse large B cell lymphoma after anti-CD19 chimeric antigen receptor T cell therapy. *Mol Ther*. 2017;25:2245–53.
13. Vedvyas Y, Shevlin E, Zaman M, Min IM, Amor-Coarasa A, Park S, et al. Longitudinal PET imaging demonstrates biphasic CAR T cell responses in survivors. *JCI Insight*. 2016;1:e90064.
14. Mailankody S, Ghosh A, Staehr M, Purdon TJ, Roshal M, Halton E, et al. Clinical responses and pharmacokinetics of MCAHR171, a human-derived bcma targeted CAR T cell therapy in relapsed/refractory multiple myeloma: final results of a phase I clinical trial. *Blood*. 2018;132:7559.
15. Kim JE, Kalimuthu S, Ahn B-C. In vivo cell tracking with bioluminescence imaging. *Nuc Med Mol Imaging*. 2015;49:3–10.
16. Ahrens ET, Bulte JW. Tracking immune cells in vivo using magnetic resonance imaging. *Nat Rev Immunol*. 2013;13:755–63.
17. Srinivas M, Aarntzen E, Bulte J, Oyen W, Heerschap A, De Vries I, et al. Imaging of cellular therapies. *Adv Drug Deliv Rev*. 2010;62:1080–93.
18. Kircher MF, Gambhir SS, Grimm J. Noninvasive cell-tracking methods. *Nat Rev Clin Oncol*. 2011;8:677–88.
19. Wang F, Wang Z, Wang F, Dong K, Zhang J, Sun YJ, et al. Comparative strategies for stem cell biodistribution in a preclinical study. *Acta Pharmacol Sin*. 2019;41:572–80.
20. Gainey MA, Siegel JA, Smergel EM, Jara BJ. Indium-111-labeled white blood cells: dosimetry in children. *J Nucl Med*. 1988;29:689–94.
21. Djekidel M, Brown RK, Pierr M. Benefits of hybrid SPECT/CT for ^{111}In -oxine-and Tc-99m-hexamethylpropylene amine oxime-labeled leukocyte imaging. *Clin Nucl Med*. 2011;36:e50–e6.
22. Charoenphun P, Meszaros LK, Chuamsaamarkkee K, Sharif-Paghaleh E, Ballinger JR, Ferris TJ, et al. [^{89}Zr] Oxinate 4 for long-term in vivo cell tracking by positron emission tomography. *Eur J Nucl Med Mol Imaging*. 2015;42:278–87.
23. Weist MR, Starr R, Aguilar B, Chea J, Miles JK, Poku E, et al. PET of adoptively transferred chimeric antigen receptor T cells with ^{89}Zr -oxine. *J Nucl Med*. 2018;59:1531–7.
24. Sato N, Wu H, Asiedu KO, Szajek LP, Griffiths GL, Choyke PL. ^{89}Zr -oxine complex PET cell imaging in monitoring cell-based therapies. *Radiology*. 2015;275:490–500.
25. Sato N, Stringaris K, Davidson-Moncada JK, Reger R, Adler SS, Dunbar C, et al. In vivo tracking of adoptively transferred natural killer-cells in rhesus macaques using ^{89}Zr -conium-oxine cell labeling and PET imaging. *Clin Cancer Res*. 2020;26:2573–81.

26. Keu KV, Witney TH, Yaghoubi S, Rosenberg J, Kurien A, Magnusson R, et al. Reporter gene imaging of targeted T cell immunotherapy in recurrent glioma. *Sci Transl Med.* 2017;9:eaag2196.
27. Lacroix S, Egrise D, Van Simaey G, Doumont G, Monclus M, Sherer F, et al. [¹⁸F]-FBEM, a tracer targeting cell-surface protein thiols for cell trafficking imaging. *Contrast Media Mol Imaging.* 2013;8:409–16.
28. Minn I, Huss DJ, Ahn H-H, Chinn TM, Park A, Jones J, et al. Imaging CAR T cell therapy with PSMA-targeted positron emission tomography. *Sci Adv.* 2019;5:eaaw5096.
29. Man F, Lim L, Volpe A, Gabizon A, Shmeeda H, Draper B, et al. In vivo PET tracking of ⁸⁹Zr-labeled Vγ9Vδ2 T cells to mouse xenograft breast tumors activated with liposomal alendronate. *Mol Ther.* 2019;27:219–29.
30. Socan A, Petrik M, Peitl PK, Krošelj M, Rangger C, Novy Z, et al. On-cartridge preparation and evaluation of ⁶⁸Ga-, ⁸⁹Zr- and ⁶⁴Cu-precursors for cell radiolabelling. *Nucl Med Biol.* 2019;71:23–31.
31. Sellmyer MA, Richman SA, Lohith K, Hou C, Weng CC, Mach RH, et al. Imaging CAR T cell trafficking with eDHFR as a PET reporter gene. *Mol Ther.* 2020;28:42–51.
32. Emami-Shahri N, Foster J, Kashani R, Gazinska P, Cook C, Sosabowski J, et al. Clinically compliant spatial and temporal imaging of chimeric antigen receptor T-cells. *Nat Commun.* 2018;9:1081.
33. Krekorian M, Fruhwirth GO, Srinivas M, Figdor CG, Heskamp S, Witney TH, et al. Imaging of T-cells and their responses during anti-cancer immunotherapy. *Theranostics.* 2019;9:7924.
34. Roesch F, J Riss P. The renaissance of the ⁶⁸Ge/⁶⁸Ga radionuclide generator initiates new developments in ⁶⁸Ga radiopharmaceutical chemistry. *Curr Top Med Chem.* 2010;10:1633–68.
35. Srivastava S, Riddell SR. Engineering CAR-T cells: design concepts. *Trends Immunol.* 2015;36:494–502.